

# Investigation of mechanical and superconducting properties of iron diffusion-doped *Bi-2223* superconductors

O. Ozturk · H. A. Cetinkara · E. Asikuzun ·  
M. Akdogan · M. Yilmazlar · C. Terzioglu

Received: 6 January 2011 / Accepted: 5 March 2011 / Published online: 17 March 2011  
© Springer Science+Business Media, LLC 2011

**Abstract** The mechanical and superconducting properties of the Fe diffusion-doped (Bi-Pb)-2223 superconductor have been investigated. First, iron was evaporated on *Bi-2223* superconductor and then the Fe layered superconductor was annealed at 830 °C for 10, 30 and 60 h. Static Vickers hardness, dc electrical resistivity, X-ray diffraction and scanning electron microscopy have been carried out to assess the effects of Fe doping. These measurements indicates that Fe doping, in comparison with the undoped samples, increased the critical transition temperature, and improved formation of high  $T_c$  phase, while decreasing the number and size of voids. Moreover, both microhardness and grain size were also enhanced by increasing the amount of diffusion. The values of microhardness were found to be load dependent. In addition, we have investigated the indentation size effect (ISE) behavior using some models such as the Kick's law, modified proportional specimen resistance (MPRS) model and the Hays- Kendall (HK) approach. Among them, both HK and MPRS models are successful. In this study, the

possible reasons of noticed improvement on mechanical and physical properties due to iron diffusion are discussed.

## 1 Introduction

Since high temperature superconductor (HTSC) was discovered, weak link behavior of grain boundaries has become one of the most important research topics [1–7]. The relationship between grain boundary structure and supercurrent conductivity could not be fully understood. Besides, the size of particles, their angles with each other, the chemical composition of grain boundaries and the volume fracture of micro-space in the sample depend on the production parameters [8, 9]. Properties of bismuth-based superconducting materials are extremely sensitive to the starting chemical rates. The starting chemical rate, rich in Bi- Pb is important as it makes up for the losses during annealing process. On the other hand, during the mechanical operating, the cracks in ceramic superconducting core are lost more easily and improve performance in samples where percentage of Pb is high. SEM measurement provides very important contribution to examine the relationship between material structure and properties [10].

Critical current density in high temperature superconductors depends on both flux and the weak link in the grain [11]. The appropriate doping of grains is a method that optimizes the transmission properties of grain boundaries in HTSC. Thus, the critical current density increased significantly and the normal state conductivity reduces significantly [12].

Mechanical properties of alloys may be determined by methods such as tension test, bending test and microhardness measurement. Changing the proportion of alloy elements and annealing applications may change the mechanical

---

O. Ozturk · E. Asikuzun  
Department of Physics, Faculty of Arts and Science, Kastamonu  
University, 37100 Kastamonu, Turkey

H. A. Cetinkara  
Department of Physics, Faculty of Arts and Science, Mustafa  
Kemal University, 31034 Hatay, Turkey

M. Akdogan · C. Terzioglu (✉)  
Department of Physics, Faculty of Arts and Science, Abant Izzet  
Baysal University, 14280 Bolu, Turkey  
e-mail: terzioglu\_c@ibu.edu.tr

M. Yilmazlar  
Faculty of Education, Sakarya University, 54300 Hendek,  
Sakarya, Turkey

properties significantly. In addition, mechanical properties may be related to the direction due to production methods [13].

The determination of mechanical properties of these alloys and development of this feature are important in choosing the application field of these alloys. Mechanical properties such as hardness, elastic modulus, yield strength, fracture toughness, brittleness index, ductility as well as the critical temperature, the critical current density and the critical magnetic field, are as important as superconducting parameters for industrial applications of high-temperature oxide superconductors [14–20]. The Vickers microhardness test is one of the convenient methods to estimate the mechanical properties. Using this method, the relationship between Vickers hardness, elastic modulus, yield strength and fracture toughness for polycrystalline superconductors at room temperature has been studied by several authors [16, 18, 21].

In this study, the effects of Fe diffusion-doped on mechanical and superconducting properties of BSCCO ceramics have been investigated. Moreover, the aim of this study is to examine the load dependence of apparent hardness and to determine load independent hardness values of the samples by using different models. In addition, X-ray diffraction and scanning electron microscopy measurements were performed to investigate the surface microstructure and surface morphology of the samples considered.

## 2 Experimental details

### 2.1 Sample preparation

Superconducting  $\text{Bi}_{1.8}\text{Pb}_{0.35}\text{Sr}_{1.9}\text{Ca}_{2.1}\text{Cu}_3\text{O}_y$  samples were prepared by the standard solid-state reaction method. The weighed powders of  $\text{Bi}_2\text{O}_3$  (99.99%),  $\text{PbO}$  (99.9 + %),  $\text{SrCO}_3$  (99.9 + %),  $\text{CaCO}_3$  (99 + %) and  $\text{CuO}$  (99 + %) in the cation ratio of  $\text{Bi}:\text{Pb}:\text{Sr}:\text{Ca}:\text{Cu} = 1.8:0.35:1.9:2.1:3$  were mixed by grinding machine for 24 h. After milling, the mixed powders were calcined in air at 700, 750 and 800 °C for 24 h. At every calcined temperature, the sample cooled to room temperature to regrind. The calcined material was reground and pressed into pellets of  $10 \times 4 \times 2 \text{ mm}^3$  at 300 MPa. The pellets were sintered in air at 830 °C for 48 h and then cooled down to room temperature. The heating and cooling rates of the temperature were chosen to be 10 and 3 °C  $\text{min}^{-1}$ , respectively. The Fe evaporation (thickness of about 50  $\mu\text{m}$ ) on one face of the samples was carried out. Then, the Fe layered superconducting samples were annealed at 830 °C for 10, 30 and 60 h. At the end of this run, Fe diffusion was realized through the samples. For comparison, an undoped

sample was also annealed under the same conditions. The samples of *Bi-2223* tablets will be hereafter denoted as F0 (undoped sample annealed at 830 °C for 10 h), F1 (iron diffused sample annealed at 830 °C for 10 h), F2 (iron diffused sample annealed at 830 °C for 30 h), and F3 (iron diffused sample annealed at 830 °C for 60 h).

### 2.2 Measurement techniques

The measurements of dc resistivity were performed with the four-probe method on all samples. Both voltage and current contacts were made with silver paint. We measured temperature (90–130 K) dependence of resistivity of the samples running 5 mA dc current through the samples in the cryostat using a Keithley 220 programmable current source and a Keithley 2182A nano-voltmeter. The transition temperature,  $T_c$ , was defined as  $R = 0$ .

X-ray diffraction (XRD) data were taken using a Rigaku D/Max-III C diffractometer with  $\text{CuK}_\alpha$  radiation in the range  $2\theta = 4^\circ\text{--}60^\circ$  with a scan speed of  $3^\circ/\text{min}$  and a step increment of  $0.02^\circ$  at room temperature. The XRD measurements provide data about lattice parameters for only a thin surface layer of Fe-diffused  $\text{Bi}_{1.8}\text{Pb}_{0.35}\text{Sr}_{1.9}\text{Ca}_{2.1}\text{Cu}_3\text{O}_y$  sample, since the effective penetration depth of the X-rays is about 15  $\mu\text{m}$  into the sample. Phase purity and the lattice parameters were determined from these XRD patterns. The mean values of lattice parameter  $c$  of  $\text{Bi}_{1.8}\text{Pb}_{0.35}\text{Sr}_{1.9}\text{Ca}_{2.1}\text{Cu}_3\text{O}_y$  samples are determined from the high-angle (00  $l$ ) peaks of the XRD measurements. The relative volume fractions of the *Bi-2223* and *Bi-2212* phases were determined from the peak intensities of the same particular reflections, using the well-known expressions [22, 23].

The surface morphologies of the Fe-diffused and pure samples were studied by using a Philips XL30 SFEG Scanning Electron Microscopy (SEM).

Hardness measurements of BSCCO samples were performed with a digital microhardness tester (Instron Series 2100) at room temperature. A Vickers pyramidal indenter with different loads (0.245, 0.490, 0.980, 1.960, and 2.940 N) and a single loading time of 10 s were applied and the diagonals of indentation were measured with an accuracy of  $\pm 0.1 \mu\text{m}$ . Indentations were made at different parts of the samples' surface such that the distance between any two indentations was more than two times the diagonal of the indentation mark to avoid surface effects due to neighboring indentation. An average of 10 readings at different locations of specimen surfaces was taken to obtain reasonable mean values for each load.

Conventional Vickers microhardness measurements consist of applying a load  $F$  on the test material via a geometrically defined indenter and after the indenter is removed, measuring the characteristic dimension,  $d$ , of the resultant impression. The Vickers microhardness,  $H_v$ , was

estimated from the average value of such indentations using the equation from Ref. [24].

$$H_v = 1.8544 \left( \frac{F}{d^2} \right) \tag{1}$$

Here  $F$  is the load applied (in N) and  $d$  the mean diagonal length of the indentation impression (in  $\mu\text{m}$ ). The scatter in the values of  $d$  did not exceed 3%.

### 3 Results and discussion

#### 3.1 XRD characterization

Figure 1 indicates the intensity as a function of  $2\theta$  for the F0, F1, F2 and F3 samples. Some of the ( $hkl$ ) peaks are indexed. The determined lattice parameters from the ( $hkl$ ) peaks of the XRD data are given in Table 1. The diffusion of Fe was indicated by an increase of the lattice parameter  $c$  of the sample in comparison with that for the undoped sample (F0). This finding is in agreement with a previous study [15]. The increase in lattice parameter  $c$  revealed that  $\text{Bi}^{3+}$ ,  $\text{Sr}^{2+}$ ,  $\text{Ca}^{2+}$  atoms might have been partly substituted by Fe atoms. The observed increase of  $T_c$  for the samples, as will be confirmed later on by dc resistivity measurements, makes the substitution at the Cu site less likely.

The calculated relative volume fraction of the samples by using well-known expressions [22, 23] is summarized in

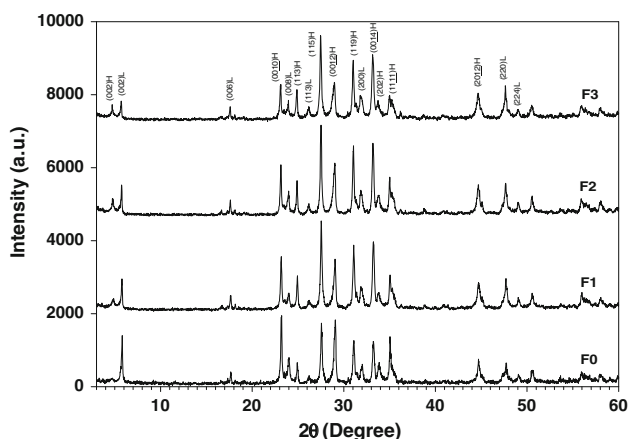


Fig. 1 XRD measurements of F0, F1, F2 and F3 powder samples

**Table 1** Critical temperature  $T_c$ , lattice parameters  $a$  and  $c$ , and volume fraction of the samples

Samples	$T_c^{offset}$ (K)	% $V_{2223}$	% $V_{2212}$	$a$ (°Å)	$c$ (°Å)
F0	100.0 ± 0.2	66.00	34.00	5,431	36.96
F1	106.0 ± 0.2	74.30	25.70	5,391	37.00
F2	106.5 ± 0.2	81.70	18.30	5,380	37.10
F3	107.0 ± 0.2	88.20	11.80	5,373	37.16

Table 1. As seen in the table, the volume fraction of  $Bi-2223$  phase increased and that of  $Bi-2212$  phase decreased with increasing Fe diffusion. The diffusion doping of the sample by iron improves formation of the high- $T_c$   $Bi-2223$  phase when compared with undoped sample. This is in conformity with the offset transition temperature of 107 K. This behaviour may be explained that the Fe doping might have not only acted as a flux but also partially replaced the  $\text{Bi}^{3+}$ ,  $\text{Sr}^{2+}$ ,  $\text{Ca}^{2+}$  ions as indicated by increasing lattice parameter  $c$ .

#### 3.2 SEM analysis

To determine the grain sizes and possible precipitation at the grain boundaries, the structure of surface morphology of the iron doped Bi (Pb)-Sr-Ca-Cu-O samples was studied by SEM Fig. 2 represents surface micrographs for the F0, F1, F2 and F3 samples. The undoped (F0) sample is composed of flake-type grains and the composition of flake-type grains is approximately equal to the  $Bi-2212$  phase [18, 25]. From the figure, we can conclude that the grains in the F0 sample are oriented randomly and poorly connected. The grain size of the F3 sample is relatively bigger than that of the F0 sample. The surface of the F3 sample is smoother and denser. In the sample F3, the flake-like grains are less dominant with respect to the sample F0, while the concentration of the needle-like grains grew gradually. The needle-like grains are believed to be due to the  $Bi-2223$  phase [18, 25, 26]. These results are in agreement with our XRD examinations and indicate that the surface morphology of the sample is relatively improved by Fe-doping. F0 has non-uniform surface appearance with smaller grains. Iron film on the sample forms a metallic connection; this resistive short-circuit connects the grains and lowers the room temperature resistivity as will be confirmed later on by dc resistivity measurements. This effect continues even when iron film is diffused into the sample, indicating the iron’s effect on grain boundary properties. SEM pictures show better connectivity in iron coated samples after heat treatment at 830 °C for 10 h. The improvement of mechanical characteristics is due to the fact that Fe can fill the intergrain spaces, and thereby reinforces the coupling between granules. From the above results, in agreement with our XRD results, it is comprehended that the Fe doped has a positive effect of decomposing the structure of the low- $T_c$  phase ( $Bi-2212$ ) and enhancing the high- $T_c$  phase ( $Bi-2223$ ) formation.

#### 3.3 Electrical measurements

The electrical resistivity was measured by using the standard four-probe dc technique, in the temperature range

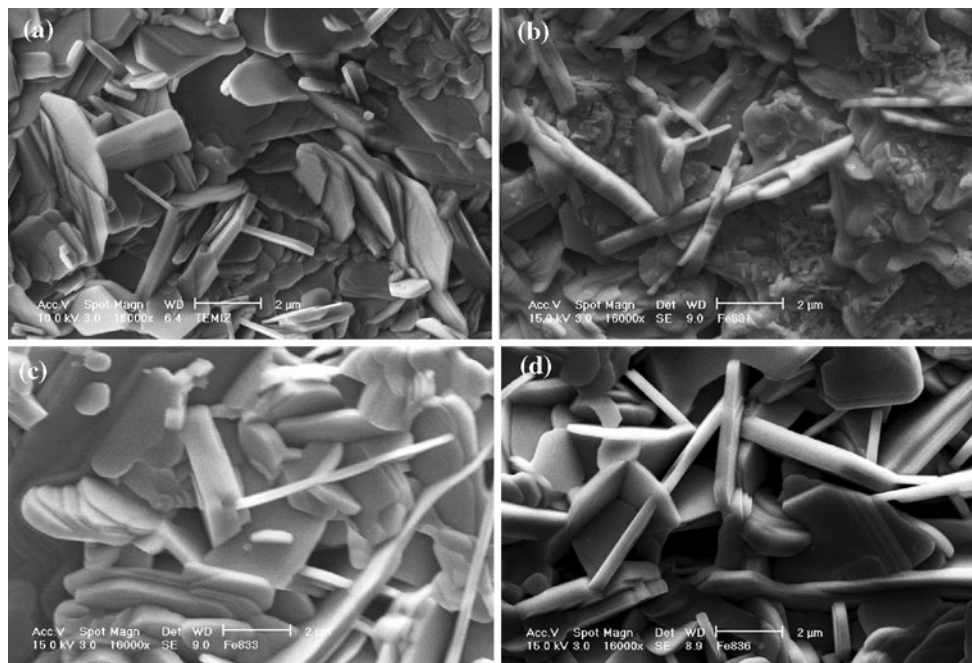


**Fig. 2** SEM measurements of the **a** F0, **b** F1, **c** F2, **d** F3 samples

between 90 and 130 K. The dc electrical resistivity as a function of temperature of F0, F1, F2 and F3 samples is shown in Fig. 3. It was observed that the value of the resistivity at room temperature decreased upon Fe doping and diffusion-annealing time. The temperature dependence of the resistivities of the samples shows the metallic behaviour in the normal state (at  $T \geq 110$  K) with the zero-resistivity transition temperatures of  $100.0 \pm 0.2$  K for F0,  $106.0 \pm 0.2$  K for F1,  $106.5 \pm 0.2$  K for F2 and  $107.0 \pm 0.2$  K for F3 sample. It can also be seen from this figure that, the normal state resistivity regularly decreases as increasing iron diffusing-doped and the tail regime clearly visible in the  $\rho$ - $T$  curve of the sample F0 [27]. In the figure, one can observe a broadening behaviour of the sample F0 with onset temperature of 108 K. The broadening reduced gradually with increasing diffusion-annealing time, in other words with increasing iron doping. The broadening of the transition width shows that F0 sample has lower percentage of the high- $T_c$  phase compared to that of iron doped samples (F1, F2 and F3). The reduction in the broadening behaviour in the  $\rho$ - $T$  curve may be due to the modifying effect of the iron doping on the grain boundaries. Sharper transitions are accompanied by higher critical temperature values. This fact suggests that somehow iron doping also affects intra-grain region. It was also observed that the transition curve of the F0 sample from the normal to the superconducting state indicates a double step transition, confirming the dominance of the low- $T_c$  phase, as seen in Fig. 1. We believe that the double step resistive

transition is an indication of weak links [27]. It is observed that the zero resistivity transition temperature of the F1 (106 K) is higher than that for the F0 sample (100 K). This is consistent with a previous work [15, 28, 29]. The increase in  $T_c$  may be related to the optimization of the hole concentration and possible changes in the lattice vibration of Bi(Pb)-Sr-Ca-Cu-O. It is also possible that resistive nature of the grain boundaries is modified by accumulation of iron atoms at the grain boundaries. This resistive short circuit of grain boundaries may eliminate the resistive tail in the  $\rho$ - $T$  curve. The results obtained from the dc resistivity as a function of temperature measurements are given in Table 1.

### 3.4 Mechanical measurements

A series of hardness measurements were attempted on the samples using indentation loads between 0.245 and 2.94 N with the help of a Vickers hardness tester. The Vickers microhardness values of different applied loads were calculated by using Eq. (1). The value of microhardness is found to change from 0.458 to 0.239 GPa in the applied load range of 0.245–2.940 N for the F0 sample. That of F1, F2 and F3 were calculated in the range of 0.529–0.302, 0.575–0.315 and 0.672–0.359 GPa, respectively. Figure 4 shows the variation of microhardness versus the applied load for the F0, F1, F2, and F3 samples. The variation of microhardness with applied load is similar in all samples as can be seen in Fig. 4. The calculated microhardness decreases rapidly with

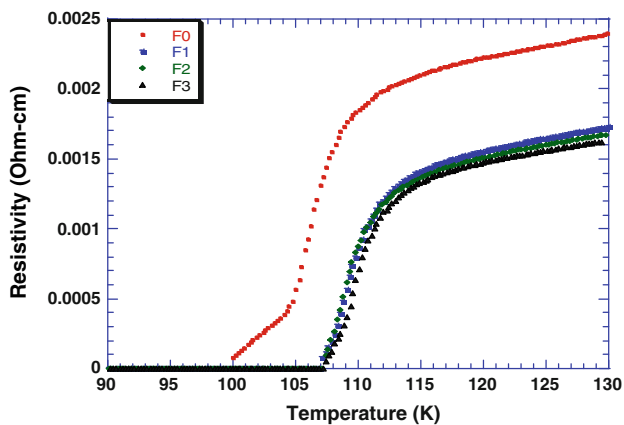


**Fig. 3** Resistivity as a function of temperature measurements of F0, F1, F2 and F3 samples

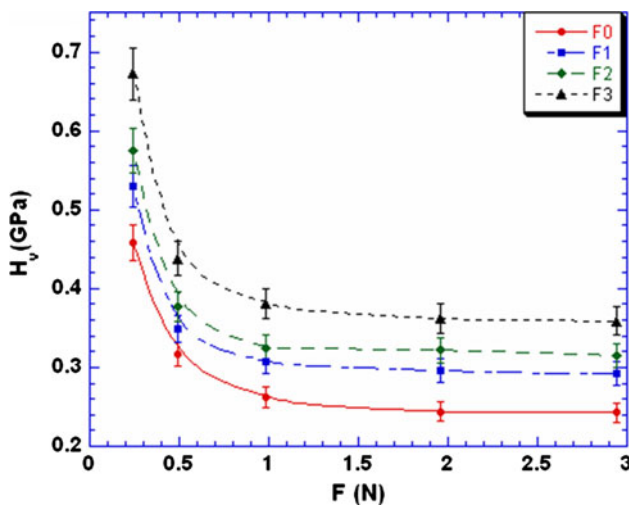


**Fig. 4** Vickers microhardness versus applied indentation load

increasing load up to 2 N and remains nearly constant thereafter. It is also observed that the microhardness values increased with increasing diffusion-annealing time. The reason of this is ascribed to Fe doping (diffusion) being able to fill the intergrain space, and leading to a remarkable increase in the mechanical resistance of the samples. Figure 2 shows a denser microstructure confirming this conclusion. It was observed that Vickers hardness increased with increasing amount of doping in *Bi-2223* superconductors [16, 18, 21]. The rapid variation of microhardness was observed with increasing applied load from 0.245 to 2.000 N. The reason for this behavior is due to the contribution of weak grain boundaries and to the process of crack formation along grain boundaries [30]. A similar result was observed for Bi-Pb-Sr-Ca-Cu-O samples [18, 20, 21] and is known as indentation size effect (ISE) [31–34]. The ISE behavior was explained qualitatively on the basis of penetration dept of the indenter [14]. The indenter gives

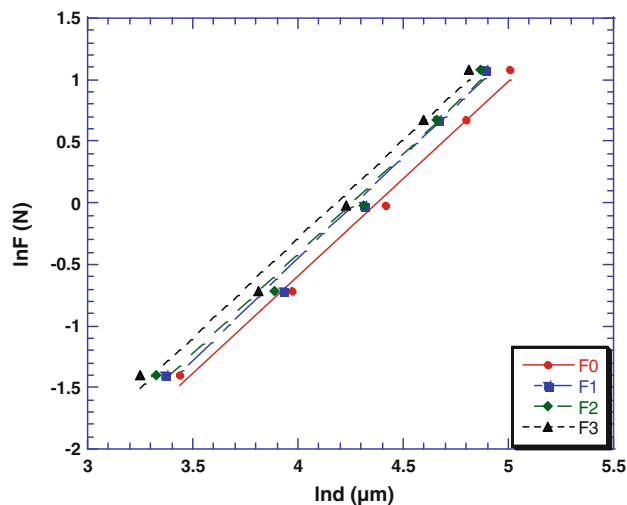


**Fig. 5** Variation of applied load  $\ln F$  with diagonal  $\ln d$  for the samples of F0, F1, F2 and F3

geometrically similar indentation; hence it follows that the measured hardness must be independent of the applied load. However, it has been well known that for many materials, microhardness calculated using Eq. (1) is load dependent as can be seen in the present work. In general, higher applied loads lead to lower hardness values. This phenomenon is known as the indentation size effect (ISE) [35].

In order to find an explanation for this effect, several relationships between the applied load and the resulting indentation size have been proposed [36–39]. Meyer’s law can be used to explain the ISE behavior of our samples [24, 32, 33, 36].

$$F = Ad^n \tag{2}$$

where the power  $n$  is the Meyer number, and  $A$  is the standard hardness constant. The value of  $n$  is used as a measure of ISE. When  $n < 2$ , the hardness increases with decrease of the applied load. The hardness increases with increasing the applied load when  $n > 2$ . When  $n_k = 2$ , the hardness is independent of applied load and is given by  $F = A_{1K}d^2$  (Kick’s law). In most cases, Kick’s law is hardly met because the exponent  $n$  is less or larger than 2. Figure 5 represents the plots of  $\ln F$  versus  $\ln d$  for the samples. Each set of the data does not show an excellent linear relationship. The slope of the graph is proportional to  $n_k$  and that of vertical intercept is proportional to  $A_{1K}$ . Through linear regression analyses, the values of  $n_k$ ,  $A_{1K}$  and  $R$  (the regression coefficient) were determined and the results are tabulated in Table 2. As can be seen from the table, it was observed that the value of the regression coefficient for each sample was found to be low,  $R < 0.99702$ , and that of  $n_k$  is less than 2. According to our results ( $n < 2$ ), our samples do not obey Kick’s law.

**Table 2** Best-fit results of experimental data according to Eq. (2)

Samples	Meyer number $n_K$	$\ln A_{1K}$ (GPa)	Regression of coefficient (R)
F0	1.583	-6.931	0.99702
F1	1.658	-7.100	0.99531
F2	1.625	-6.922	0.99485
F3	1.603	-6.714	0.99565

In order to explain the ISE behavior, a modified PSR (MPSR) model has recently been suggested [39]. According to this modified model.

$$F = W_{MPSR} + A_{0MPSR}^d + A_{1MPSR}^{d^2} \tag{3}$$

here  $W_{MPSR}$  corresponds to minimum applied load to produce an indentation,  $A_{0MPSR}$  and  $A_{1MPSR}$  are related to the energies dissipated for creating a new surface of a unit area and for producing the permanent deformation of a unit volume, and is a measure of the load independent hardness estimated by MPSR model, respectively. Figure 6 shows  $F$  versus  $d$  graph for the samples. From a conventional polynomial fit of this expression (Eq. 3) to the data, the parameters of  $W_{MPSR}$ ,  $A_{0MPSR}$ ,  $A_{1MPSR}$  and  $R$  were extracted for all samples and tabulated in Table 3. According to the

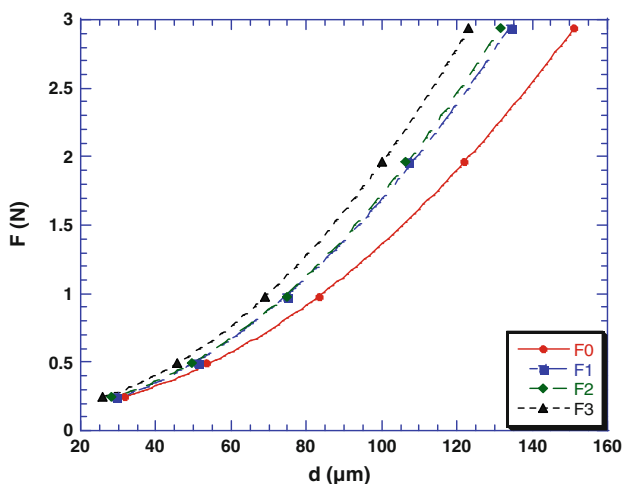


**Fig. 6** Variation of applied load with the indentation diagonal length for the samples of F0, F1, F2 and F3

**Table 3** Best-fit results of experimental data according to Eqs. (3) and (4)

Samples	$W_{MPSR}$ (N)	$A_{0MPSR}$ (N/ $\mu\text{m}$ )	$A_{1MPSR}$ (N/ $\mu\text{m}^2$ )	Regression of coefficient (R)	Load independent hardness $H_{LMPSR}$ (GPa)	Load dependent hardness (in plateau regime) $H_v$ (GPa)
F0	0.129	$-2.46 \times 10^{-5}$	$12.33 \times 10^{-5}$	0.99998	0.228	0.239–0.244
F1	0.081	$45.1 \times 10^{-5}$	$15.60 \times 10^{-5}$	0.99974	0.289	0.302–0.315
F2	0.155	$-191 \times 10^{-5}$	$17.60 \times 10^{-5}$	0.99992	0.326	0.315–0.321
F3	0.159	$-180 \times 10^{-5}$	$19.80 \times 10^{-5}$	0.99999	0.367	0.359–0.361

MPSR model, the load independent hardness can be calculated by relation,

$$H_{LMPSR} = \left( A_{1MPSR} / 26.43 \right) \tag{4}$$

The calculated load independent hardness for each sample is listed in Table 3. J. B. Quinn and G. D. Quinn [40]. examined the variation of Vickers microhardness as a function of indentation load for a variety of ceramic materials. They observed that such hardness-load curve shows distinct transition to a plateau of the constant hardness level and concluded that the transition in such curves correspond to the intrinsic hardness value of the material. In this study, this plateau is reached at 2 N applied load for the samples. As can be seen from the table, load independent microhardness value of F0 sample (0.228 GPa) is lower than the hardness results (see Fig. 4) in the plateau region ( $H_v = 0.239$  and 0.244 GPa). This value is close to the hardness of the measured with the load 0.249 N which is not in plateau region.

Hays and Kendal (HK) [38] proposed a concept that there exist minimum levels of the applied test load,  $W_{HK}$ , named minimum applied load to produce an indentation for the purpose of examining the ISE in our samples. They introduced an effective indentation load,  $F_{eff} = F - W_{HK}$ , and proposed the following relationship (modified Kick’s law),

$$F - W_{HK} = A_{1HK}d^2 \tag{5}$$

where  $A_{1HK}$  is the load independent hardness constant calculated by HK approach for a given sample. Figure 7 exhibits applied load as a function of the square of the impression semidiagonal for the samples. Each set of data shows an excellent linear relationship ( $R > 0.99914$ ). The slope of each line corresponds to the load independent hardness constant,  $A_{1HK}$  and the intercept of each line represents the sample resistance pressure,  $W_{HK}$ . The extracted values of  $W_{HK}$ ,  $A_{1HK}$  and  $R$  were listed in Table 4. As can be seen from the table, it was observed that the values of  $W_{HK}$  and  $A_{1HK}$  of the samples increased with increasing the diffusion-annealing time and the regression coefficient of each sample is very high, implying that Eq. (5) provides a satisfactory description of the indentation data for the samples. Figure 8 exhibits a plot

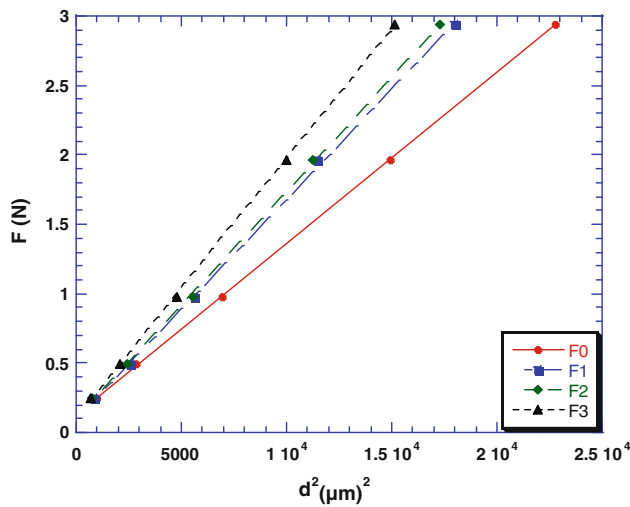


**Fig. 7** Applied load as a function of the square of the impression semidiagonal for the samples of F0, F1, F2 and F3

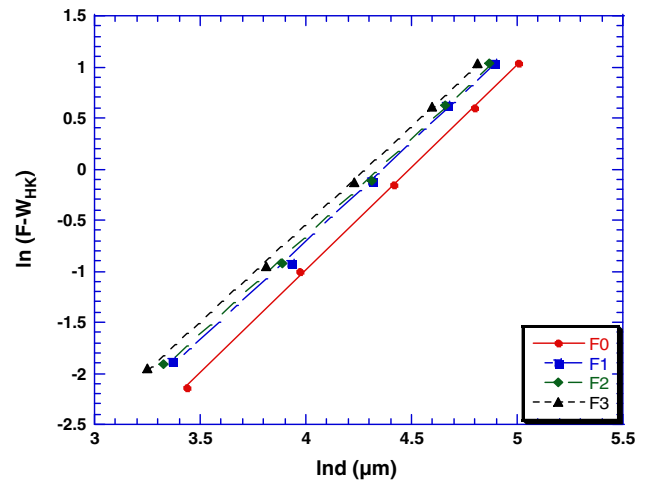


**Fig. 8** Relationship between true applied load  $\ln(F-W_{HK})$  and the Vickers diagonal  $lnd$  for the samples of F0, F1, F2 and F3

of  $\ln(F-W_{HK})$  versus  $lnd$  and gives a value of  $n_{HK} \approx 2$  (see Table 4) for all samples. This result confirms the validity of Eq. (5) or HK law in the explanation of the dependence of microhardness on applied load. According to the HK approximation, load independent microhardness  $H_{LHK}$  can be calculated by relation.

$$H_{LHK} = 1.8544A_{1HK}. \tag{6}$$

The values of  $H_{LHK}$  were calculated by using Eq. (6) and summarized in Table 4. The load independent hardness values estimated by HK approach ( $H_{LHK} = 0.228$  GPa) and the hardness results of F0 sample (see Fig. 4) in the plateau region ( $H_v = 0.239$  and  $0.244$  GPa) are comparable. This behavior is observed in other samples (F1, F2 and F3) of this work. The HK approach also provides a satisfactory description for measured indentation data.

The load independent values  $H_{LHK}$ ,  $H_{LMPSR}$  calculated by HK approach and MPSR model are obviously closer to plateau value. We may therefore, suggest that both the  $H_{LHK}$  and  $H_{LMPSR}$  values are convenient and correspond to the intrinsic hardness values of the samples.

We have investigated variation in the hardness of the Bi(Pb)-Sr-Ca-Cu-O ceramic material depending on doping and substitution concentration [16–18]. It was observed

that the hardness of doped Bi (Pb)-Sr-Ca-Cu-O samples is greater than that of undoped ones. This may be due to both pinning of dislocations at the impurity sites and other defects caused by the presence of impurity atoms in the crystal, and also to variation in the magnitude of the bond forces in the crystal containing impurities [14]. In the present work, the load independent microhardness increased in Fe doped samples. It also increased with increasing diffusion-annealing time for Fe doped samples. XRD analysis showed the formation of the high- $T_c$  phase in Fe doped samples, in comparison with those of undoped samples of Bi-2223. SEM analysis indicated that both of the number and size of the voids at the surface decrease increasing the grain connectivity in Fe doped samples. The reason of the improvement in superconducting and mechanical properties of the samples is that Fe can fill the intergrain spaces, and thereby reinforce the coupling between granules. From the above results, it is inferred that the Fe doped has the positive effect of decomposing the structure of the low- $T_c$  phase and enhancing the high- $T_c$  phase creation. We can conclude that the estimation of hardness values by using one applied load is not appropriate. This behavior is ascribed to the following: (I) at larger indentation loads, the Vickers hardness registered

**Table 4** Best-fit results of experimental data according to Eqs. (5) and (6)

Samples	Load independent hardness $A_{1HK}$ (GPa)	Sample resistance pressure $W_{HK}$ (N)	Regression of coefficient (R)	$n_{HK}$	Regression of coefficient (R)	Load independent hardness $H_{LHK}$ (GPa)	Load dependent hardness (in plateau regime) $H_v$ (GPa)
F0	$12.32 \times 10^{-5}$	0.128	0.99998	2.00	0.99998	0.228	0.239–0.244
F1	$15.89 \times 10^{-5}$	0.093	0.99974	1.94	0.99914	0.294	0.302–0.315
F2	$16.45 \times 10^{-5}$	0.097	0.99984	1.93	0.99924	0.305	0.315–0.321
F3	$18.63 \times 10^{-5}$	0.104	0.99993	1.92	0.99962	0.345	0.359–0.361

smaller values, this observation may be due to the presence of weak grain boundaries of the superconducting ceramics; (II) at smaller indentation loads, the Vickers hardness recorded higher values, this is ascribed to the fact that the measured hardness more indicative of the monocrystalline state without interference from the grain boundaries [18]. Therefore, the load independent hardness values are reasonable to define the entire sample hardness.

#### 4 Conclusions

Fe-doped  $\text{Bi}_{1.8}\text{Pb}_{0.35}\text{Sr}_{1.9}\text{Ca}_{2.1}\text{Cu}_3\text{O}_y$  samples prepared by solid state reaction methods are compared with those for the undoped sample. The lattice parameter  $c$ , the critical transition temperature, and the high- $T_c$  temperature ratio increased with Fe doping. Surface morphology of Fe-doped samples showed a denser microstructure. The improvement of superconducting properties due to the modification of grain boundaries by Fe doping is determined by lower normal state resistivity. We have used three different empirical models to analyze the non-linear relation between load and hardness and presented a comparison of the performance of the considered models. The estimated hardness values of the samples are load dependent. Fe doping is found to increase the hardness of the samples. Among the three empirical models used to analyze the load versus indentation data, we have found that both the HK and MPSR models are suitable for describing the experimental data.

**Acknowledgments** This work is supported partly by The Scientific and Technological Council of Turkey (Project No: 104T325) and partly by the Turkish State Planning Organization (DPT) (Project No: 2004K120200).

#### References

1. L. Pierre, J. Schneck, D. Morin, J.C. Toledona, J. Primot, C. Daguët, H. Savary, *J. Appl. Phys.* **68**, 2296 (1990)
2. R.K. Nkum, W.R. Datars, *Physica C* **190**, 465 (1992)
3. K. Nanda Kishore, M. Muralidhar, V. Hari Babu, *Physica C* **204**, 299 (1993)
4. S. Kambe, Y.C. Guo, S.X. Dou, H.K. Liu, Y. Wakahara, H. Maeda, K. Kakimoto, M. Yavuz, *Supercond. Sci. Technol.* **11**, 1061 (1998)
5. C. Terzioglu, M. Yilmazlar, O. Ozturk, E. Yanmaz, *Physica C* **423**, 119 (2005)
6. V.G. Prabitha, A. Biju, R.G. Abhilash Kumar, P.M. Sarun, R.P. Aloysius, U. Syamaprasad, *Physica C* **433**, 28 (2005)
7. C. Terzioglu, O. Ozturk, A. Kilic, A. Gencer, I. Belenli, *Physica C* **434**, 153 (2006)
8. J.W. Ko, J.M. Yoo, Y.K. Kim, K.H. Oh, S.J. Choe, H. Chung, *Cryogenics* **43**, 549–553 (2003)
9. B. Zhao, X. Wan, W. Song, Y. Sun, J. Du, *Physica C* **337**, 138–144 (2000)
10. S.E. Babcock, *Micron* **30**, 449–461 (1999)
11. J.D. Hettinger, K.E. Gray, D.J. Miller, D.H. Kim, D.G. Steel, B.R. Washburn, J. Sharping, C. Moreau, M. Eddy, J.E. Tkaczyk, J. Deluca, J.H. Kang, J. Talvacchio, *Physica C* **273**, 275–280 (1997)
12. J. Mannhart, H. Bielefeldt, B. Goetz, H. Hilgenkamp, A. Schmehl, C.W. Schneider, R.R. Schulz, *Physica C* **341–348**, 1393–1396 (2000)
13. A. Murakami, K. Katagiri et al., *Physica C* **392–396**, 557–561 (2003)
14. U. Kölemen, O. Uzun, M. Yilmazlar, N. Güçlü, E. Yanmaz, *J. Alloy. Compd.* **415**, 300–306 (2006)
15. M. Nursoy, M. Yilmazlar, C. Terzioglu, I. Belenli, *J. Alloy. Compd.* **459**(1–2), 399 (2008)
16. M. Yilmazlar, H.A. Cetinkara, M. Nursoy, O. Ozturk, C. Terzioglu, *Physica C* **442**, 101 (2006)
17. S.M. Khalil, *Smart Mater. Struct.* **14**, 804 (2005)
18. S.M. Khalil, *J. Phys. Chem. Solids* **62**, 457 (2001)
19. A. Murakami, K. Katagiri, K. Noto, K. Kasaba, Y. Sohoji, M. Muralidhar, N. Sakai, M. Murakami, *Physica C* **378–381**, 794 (2002)
20. K. Katagiri, A. Murakami, R. Kan, K. Kasaba, K. Noto, M. Muralidhar, N. Sakai, M. Murakami, *Physica C* **392–396**, 526 (2002)
21. E. Bruneel, J. Degrieck, I. Van Driessche, S. Hoste, *Physica C* **372–376**, 1063 (2002)
22. C.W. Chiu, R.L. Meng, L. Gao, Z.J. Huang, F. Chen, Y.Y. Xue, *Nature* **365**, 323 (1993)
23. S.A. Halim, S.A. Khawaldeh, S.B. Mohammed, H. Azhan, *Mater. Chem. Phys.* **61**, 251 (1999)
24. B.W. Mott, *Microindentation Hardness Testing*, vol. 9 (Butterworths, London, 1956)
25. Y.C. Chen, K.K. Chong, T.H. Meen, *Jpn. J. Appl. Phys.* **30**, L33 (1991)
26. K.H. Yoon, Y.B. Lee, *J. Mater. Sci.* **26**, 5101 (1991)
27. P. Kameli, H. Salamati, M. Eslami, *Solid State Commun.* **137**, 30–35 (2006)
28. O. Ozturk, T. Kucukomeroglu, C. Terzioglu, *J. Phys. Condens. Matter* **19**, 346205 (2007). (10 pp)
29. C. Terzioglu, O. Ozturk, I. Belenli, *J. Alloy. Compd.* **471**, 142–146 (2009)
30. H.C. Ling, M.F. Yan, *J. Appl. Phys.* **64**, 1307 (1988)
31. J. Gong, J. Wu, Z. Guan, *Mater. Lett.* **38**, 197 (1999)
32. K. Sangwal, B. Surowska, *Mater. Res. Innov.* **7**, 91 (2003)
33. R. Tickoo, R.P. Tandon, K.K. Bamzai, P.N. Kotru, *Mater. Chem. Phys.* **42**, 446 (2003)
34. A.A. Elmustafa, D.S. Stone, *J. Mech. Phys. Solid* **51**, 357 (2003)
35. O. Ozturk, C. Terzioglu, I. Belenli, *J. Supercond. Nov. Magn.* (2010). doi: [10.1007/s10948-010-0998-z](https://doi.org/10.1007/s10948-010-0998-z)
36. F. Fröhlich, P. Grau, W. Grellmann, *Phys. Status Solidi* **42**, 79 (1997)
37. H. Li, R.C. Bradt, *J. Mater. Sci.* **22**, 917 (1993)
38. C. Hays, E.G. Kendall, *Metallography* **6**(4), 275 (1973)
39. J. Gong, J. Wu, Z. Guan, *J. Eur. Ceram. Soc.* **19**, 2625 (1999)
40. J.B. Quinn, G.D. Quinn, *J. Mater. Sci.* **32**, 4331 (1997)